

Ultrashallow (<10 nm) p^+/n junction formed by $B_{18}H_{22}$ cluster ion implantation and excimer laser annealing

Sungho Heo^{a)} and Hyunsang Hwang^{b)}

Department of Materials Science and Engineering, Gwangju Institute of Science and Technology,
No. 1 Oryong-dong, Buk-gu, Gwangju 500-712, Korea

H. T. Cho and W. A. Krull

SemEquip, Inc., 34 Sullivan Road, Billerica, Massachusetts 01862

(Received 3 April 2006; accepted 8 November 2006; published online 15 December 2006)

In order to form an ultrashallow p^+/n junction, incorporation of a top amorphous-silicon (a -Si) layer is necessary so as to avoid channeling and to fully activate the dopant. Conventional ultrashallow junction processes require two-step implantation such as preamorphization by Si^+ or Ge^+ implantation and ultralow (<0.5 keV) energy B^+ implantation. In this report, the authors investigate $B_{18}H_{22}^+$ implantation. Due to the heavy mass of cluster ions, one-step ion implantation at 5 keV readily forms a 5-nm-thick a -Si layer and an ultrashallow junction without B channeling. By employing excimer laser annealing, the authors have obtained a shallow junction depth (~ 9 nm) and low R_s ($\sim 830 \Omega/\square$). © 2006 American Institute of Physics. [DOI: 10.1063/1.2405863]

Conventional B^+ and BF_2^+ implantation generally cannot satisfy the requirement of p^+/n junction depth (X_j) for sub-45 nm complementary metal-oxide-semiconductor (CMOS) devices. Ultralow energy (ULE) B^+ implantation exhibits very low throughput due to low beam current (current α energy^{3/2}).¹ For BF_2^+ implantation, the dopant activation rate normally degrades due to the presence of F.^{2,3} Although cluster B ion implantation has been studied as an alternative method, $B_{10}H_{14}^+$ (decaborane) showed limited improvement.⁴

We have studied the advantages of $B_{18}H_{22}$ (octadecaborane). $B_{18}H_{22}^+$ implantation can be employed to form an amorphous-silicon (a -Si) layer without additional ion implantation. It can also simultaneously reduce B channeling due to its 20 times higher mass relative to B.⁵ This approach offers various advantages such as high throughput, low beam divergence, and high dose implantation. However, like B^+ implantation, cluster B ion implantation also shows transient enhance diffusion (TED) during rapid thermal annealing (RTA), which increases the X_j .⁶

In this letter, we applied excimer laser annealing (ELA) to $B_{18}H_{22}^+$ implanted samples. ELA can be employed to achieve a high activation rate above the solid solubility limit and reduce TED due to the short annealing time (approximately nanoseconds).⁷ We also evaluated the effect of applying low-temperature annealing prior to ELA.

$B_{18}H_{22}^+$ ions at an energy of 5–20 keV were implanted in drift mode to an actual B dose of 3×10^{14} – $1 \times 10^{15}/\text{cm}^2$ into n -type Si substrates. The equivalent implant energy is 0.25–1 keV according to the ratio of B per cluster B mass ($1/20 = B_{\text{mass}}/B_{18}H_{22,\text{mass}}$). ELA was conducted with an energy of 300–700 mJ/cm² at one pulse. For comparison with ELA, RTA was performed at 950 °C for 10 s. Preannealing was conducted at 400–500 °C for 5 min in N_2 ambient. The sheet resistance (R_s) and active carrier concentration (N_s) were measured by the van der Pauw pattern and Hall measurement. A high-resolution cross-sectional transmission

electron microscopy (HR-XTEM) analysis was also conducted. The B dopant depth profiles were obtained by secondary ion mass spectrometry (SIMS) analysis without an O_2 leak.⁸

Figure 1 shows R_s and dopant activation rate (%) following ELA. Cluster B ion implantation generates more interstitial and vacancies in the Si substrate, resulting from high energy irradiation and a multiple collision effect.⁹ Based on these phenomena, cluster B ion implantation results in more damage and different kinds of defects in the Si substrate compared with B^+ implantation. Thus, $B_{18}H_{22}^+$ implantation yields a thick a -Si layer (~ 5 nm) equivalent to that obtained from Ge preamorphized implantation (PAI) at ~ 3 keV (inset of HR-XTEM image in Fig. 1).¹⁰ Interestingly, cluster B ion implantation creates a smooth amorphous/crystalline-Si (a/c -Si) interface in spite of generating more Si interstitials. The mechanism underlying the smooth a/c -Si interface formation is not clearly understood at present, and thus further research is necessary. Up to a laser energy of 500 mJ/cm², the R_s decreased below 830 Ω/\square , and the dopant activation rate was increased beyond 72%. This indicates that laser en-

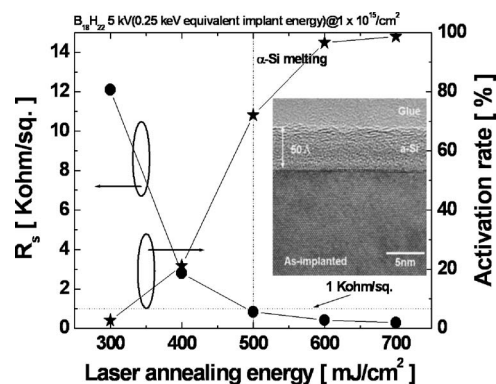


FIG. 1. Variation of sheet resistance (R_s) and activation rate (%) as a function of ELA energy of 300–700 mJ/cm² with one pulse. The inset of the HR-XTEM image shows the $B_{18}H_{22}^+$ as-implanted sample at an equivalent implantation energy of 0.25 keV with an actual dose of $1 \times 10^{15}/\text{cm}^2$. The a -Si layer thickness was 5 nm.

^{a)}Electronic mail: kojiro@gist.ac.kr

^{b)}Electronic mail: hwanghs@gist.ac.kr

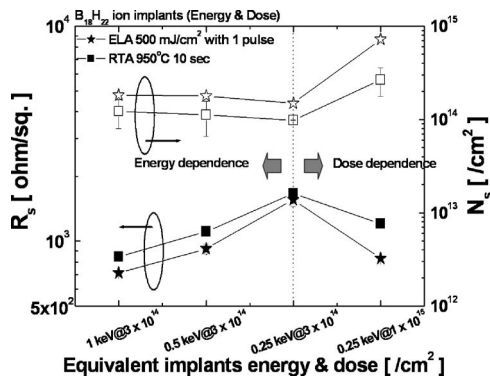


FIG. 2. Variation of R_s and N_s as a function of implanted conditions (energy and dose) with annealing methods (RTA and ELA at 500 mJ/cm²). B equivalent implantation energy was calculated by cluster ion extraction energy.

ergy above 500 mJ/cm² is sufficient for dopant activation, owing to recrystallization of the *a*-Si layer. The *a*-Si melting temperature is normally 300 °C lower than that for *c*-Si layer.¹¹ Thus the *a*-Si layer is melted by ELA at 500 mJ/cm² without melting the *c*-Si substrate. High energy ELA (>850 mJ/cm²) generally leads to deeper X_j and gate deformation in a conventional CMOS process due to melting of the *c*-Si substrate.^{12,13} The proposed approach of B₁₈H₂₂⁺ implantation with ELA at 500 mJ/cm² is expected to mitigate the problem of process integration.

The critical ELA energy is directly related to the *a*-Si thickness and implanted dose for dopant activation. Hence, we prepared various implant samples with ELA and RTA, as shown in Fig. 2. Compared with RTA, ELA shows improved R_s and N_s values. The enhancement of these parameters is attributed to dopant activation above the solid solubility limit. The sample implanted at energy of 1 keV shows lower R_s and higher N_s values after ELA than those of the control sample implanted at 0.25 keV. These changes are attributed to a deeper X_j . The high dose implanted sample shows a lower R_s value than that of the control sample without any increase in the implantation energy due to the increase of dopant activation.

In order to control *a*-Si thickness and residual defects, we applied preannealing for solid phase epitaxial regrowth (SPER) of *a*-Si prior to ELA.¹⁴ Figure 3 shows the effect of low-temperature annealing prior to ELA. With increasing preannealing temperature, R_s is also increased. This increase is attributed to a reduction in *a*-Si thickness resulting from

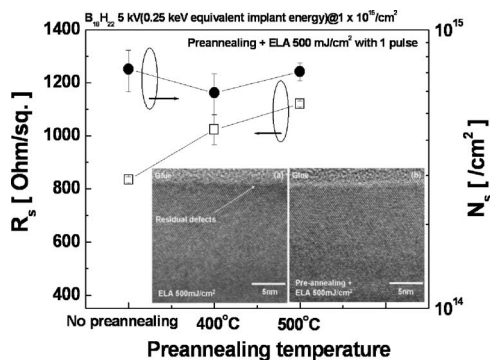


FIG. 3. Variation of R_s and N_s as a function of ELA at 500 mJ/cm² with and without preannealing. The insets of the HR-XTEM images show the sample without preannealing (a) and that with preannealing (b).

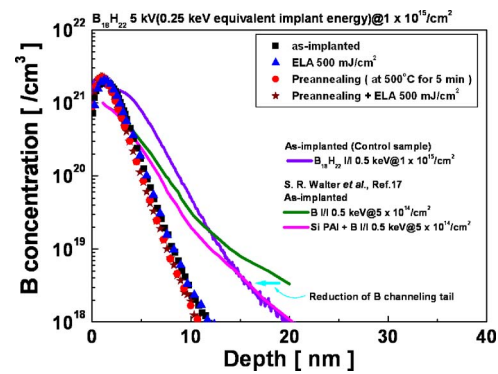


FIG. 4. (Color online) SIMS depth profile of B before and after ELA with or without preannealing. Reported results show as-implanted B SIMS depth profiles (B⁺ and Si PAI+B⁺ implantations).

the SPER process; the *a*-Si layer is then regrown in *c*-Si by ELA. The combination of preannealing and ELA yields fewer residual defects as there is sufficient annealing time to recover the residual damage [see Fig. 3(b)]. Thus sample that is preannealed prior to ELA is expected to have lower leakage current than the one-step ELA sample. However, for high R_s (~1100 Ω/□), preannealing prior to ELA is found to be ineffective in terms of achieving high dopant activation. B₁₈H₂₂⁺ implantation creates a thick *a*-Si layer with a smooth *a/c*-Si interface. This *a*-Si layer leads to a high B activation rate after one-step ELA.

Figure 4 shows the B SIMS depth profile after various process conditions as well as reported results.¹⁵ Due to self-amorphization, one-step B₁₈H₂₂⁺ implantation (control sample) can yield a X_j equivalent to that of conventional Si PAI and ULE B⁺ implantation. Lenoble *et al.*¹⁶ demonstrated that conventional ULE (<0.5 keV) B⁺ implantation suffers from various problems. They also showed that the relatively deep depth profile originates from energy contamination caused by the deceleration mode. In contrast, the B₁₈H₂₂ implanted sample at 0.25 keV has a shallower depth profile without any energy contamination. After ELA at 500 mJ/cm², diffusion of the B profile was almost negligible. This is attributed to similarities between the ELA process employed here and nonmelting laser annealing. For a channel doping concentration of 5×10^{18} /cm², X_j was 9 nm and the vertical abruptness was ~2.6 nm/decade. The preannealed sample shows a somewhat shallow depth profile. This might be attributable to inaccuracy of the SIMS analysis due to the presence of a very thin surface oxide. T. H. Buyuklimanli *et al.*⁸ reported that a higher sputtering rate in the surface oxide layer results in a shallow B depth profile and additional error in X_j . Our preannealed sample has a very thin surface oxide layer because preannealing was conducted under a low vacuum condition in N₂ ambient (working pressure: 100 mTorr), which is not sufficient to remove the residual O₂ gas. The real X_j of the preannealed sample is expected to be similar to that of the as-implanted sample. A combination of preannealing and ELA also shows negligible B diffusion.

Figure 5 shows the relationship of R_s and X_j obtained from this experiment as well as from reported results.^{3,5,17} Implantation of various dopants such as B⁺, BF₂⁺, B₁₀H₁₄⁺, and B₁₈H₂₂⁺ and various annealing methods was evaluated. Compared with reported results, the one-step ELA sample shows shallower X_j and lower R_s . We can further scale down

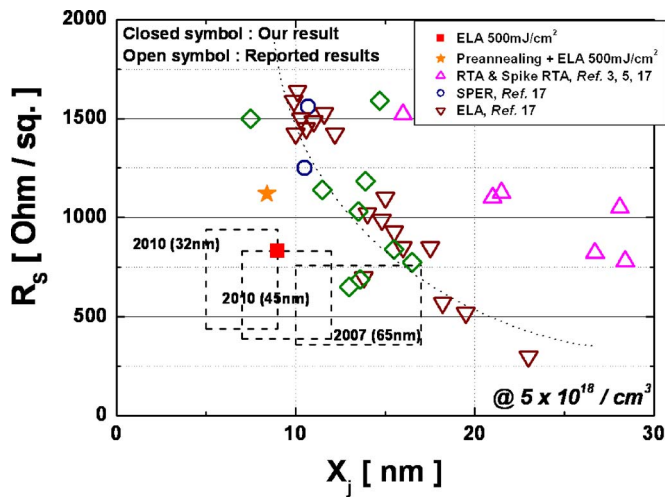


FIG. 5. (Color online) Relationship of R_s vs X_j . The closed and open symbols denote this experiment and reported results, respectively. The reported results were obtained by various annealing methods such as RTA, spike RTA, SPER, ELA, and FLA flash lamp annealing.

X_j to as shallow as 9 nm, while maintaining R_s as low as 830 Ω/\square . Considering the high R_s value, a combination of preannealing and ELA is not an appropriate annealing method for scaling down R_s - X_j .

In summary, a sub-10 nm ultrashallow p^+/n junction formed by $B_{18}H_{22}^+$ implantation and ELA is demonstrated. $B_{18}H_{22}^+$ implantation can readily produce a thick a -Si layer with a smooth a/c -Si interface, which is attributed to higher dopant activation after ELA. By employing ELA, a shallow X_j (~ 9 nm) and low R_s ($\sim 830 \Omega/\square$) can be obtained by nonmelting laser annealing. Although the combination of preannealing and ELA yields high R_s ($\sim 1100 \Omega/\square$), it is expected to reduce leakage current and result in fewer residual defects. Considering the various advantages noted here, the proposed approach of $B_{18}H_{22}^+$ implantation with one-step ELA appears to be a promising process for the sub-45 nm CMOS technology node.

The authors would like to thank J. W. Marino in Charles Evans Association for providing SIMS analysis.

- ¹X. Lu, L. Shao, X. Wang, J. Liu, W. Chu, J. Bennet, L. Larson, and P. Ling, *J. Vac. Sci. Technol. B* **20**, 992 (2002).
- ²J. Jin, J. Liu, U. Jeong, S. Mehta, and K. Jones, *J. Vac. Sci. Technol. B* **20**, 442 (2002).
- ³K. Goto, J. Matsuo, Y. Tada, T. Sugii, and I. Yamada, *IEEE Trans. Electron Devices* **46**, 683 (1999).
- ⁴D. Takeuchi, N. Shimada, J. Matsuo, and I. Yamada, *Nucl. Instrum. Methods Phys. Res. B* **121**, 345 (1997).
- ⁵Y. Kawasaki, T. Kuroi, T. Yamashita, K. Horita, T. Hayashi, M. Ishibashi, M. Togawa, Y. Ohno, M. Yoneda, T. Horsky, D. Jacobson, and W. Krull, *Nucl. Instrum. Methods Phys. Res. B* **237**, 25 (2005).
- ⁶A. Agarwal, H.-J. Gossman, D. C. Jacobson, D. J. Eaglesham, M. Sosnowski, J. M. Poate, I. Yamada, J. Matsuo, and T. E. Haynes, *Appl. Phys. Lett.* **73**, 2015 (1998).
- ⁷G. Fortunato, L. Mariucci, A. L. Magna, P. Alippi, M. Italia, V. Privitera, B. Svensson, and E. Monakhov, *Appl. Phys. Lett.* **85**, 2268 (2004).
- ⁸T. H. Buyuklimanli, C. W. Magee, J. W. Marino, and S. R. Walter, *J. Vac. Sci. Technol. B* **24**, 408 (2006).
- ⁹T. Aoki, J. Matsuo, and G. Takaoka, *Proceeding of the 14th International Conference on Ion Implantation Technology*, 2002, p. 560.
- ¹⁰B. J. Pawlak, R. Lindsay, R. Surdeanu, P. Stolk, K. Maex, and X. Pages, *Proceeding of the 14th International Conference on Ion Implantation Technology*, 2002, p. 21.
- ¹¹E. V. Monakhov, B. G. Svensson, M. K. Linnarsson, A. L. Magna, M. Italia, V. Privitera, G. Fortunato, M. Cuscunà, and L. Mariucci, *Appl. Phys. Lett.* **87**, 192109 (2005).
- ¹²E. V. Monakhov, B. G. Svensson, M. K. Linnarsson, A. L. Magna, C. Spinella, C. Bongiorno, V. Privitera, G. Fortunato, and L. Mariucci, *Appl. Phys. Lett.* **86**, 151902 (2005).
- ¹³M. Hernandez, J. Venturini, D. Zahorski, J. Boulmer, D. Débarre, G. Kerrien, T. Sarnet, C. Laviro, M. N. Semerica, D. Camel, and J. L. Santailier, *Appl. Surf. Sci.* **208**, 345 (2003).
- ¹⁴L. Csepregi, E. F. Kennedy, T. J. Gallagher, J. W. Mayer, and T. W. Sigmon, *J. Appl. Phys.* **48**, 4234 (1977).
- ¹⁵S. R. Walther, S. Mehta, J. Weeman, A. Grouillet, and D. Brown, *Proceeding of the 12th International Conference on Ion Implantation Technology*, 1998, p. 126.
- ¹⁶D. Lenoble, A. Grouillet, F. Arnaud, M. Haond, S. B. Felch, Z. Fang, S. Walther, and R. B. Liebert, *Proceeding of the 13th International Conference on Ion Implantation Technology*, 2000, p. 468.
- ¹⁷K. Suguro, T. Ito, K. Matsuo, T. Inuma, and K. T. Nishinohara, *Extended Abstracts of the fourth international Workshop on Junction Technology*, Shanghai, 15–16 March 2004, p. 18.